Morphology of Model Graft Copolymers with Randomly Placed Trifunctional and Tetrafunctional Branch Points

Maria Xenidou,[†] Frederick L. Beyer,[‡] Nikos Hadjichristidis,[†] Samuel P. Gido,*[,‡] and Nora Beck Tan[§]

Department of Chemistry, University of Athens, Panepistimiopolis Zografou 15771, Athens, Greece, Polymer Science and Engineering Department, W. M. Keck Electron Microscopy Laboratory, University of Massachusetts, Amherst, Massachusetts 01003, and Polymers Research Branch, U.S. Army Research Laboratory, Aberdeen Proving Ground, Maryland 21005-5069

Received June 1, 1998; Revised Manuscript Received August 10, 1998

ABSTRACT: The morphologies of two series of model graft copolymers were studied using transmission electron microscopy (TEM) and small-angle X-ray scattering (SAXS). Both series of materials have monodisperse polybutadiene (PB) backbones and monodisperse polystyrene (PS) graft blocks. In one series there are on average five trifunctional junction points randomly distributed along the PB backbone. Each junction point grafts one PS block to the backbone. In the other series there are on average four tetrafunctional junction points randomly distributed along the PB backbone. Each junction point grafts two PS blocks to the backbone. A range of overall PB and PS volume fractions was investigated for both series. These materials simulate a controlled and known degree of architectural disorder. Current theory cannot rigorously predict the morphological behavior for these complex molecular architectures. However, it is found that an approximate extension of existing theory utilizing the constituting block copolymer (fundamental building block) concept allows a rational explanation of the effect of architecture on morphology in these materials. The materials form the domain shape (spheres, cylinders, or lamellae) which is predicted by theory, but spherical and cylindrical morphologies lack the long-range lattice order found in diblocks and other simpler block copolymer molecular architectures. When lamellar morphologies are formed, however, at least some long range order is always present due to the space filling requirements of the lamellar domains.

Introduction

This paper reports morphological characterization results for two model series of architecturally well defined graft copolymers with polybutadiene (PB) backbones and polystyrene (PS) grafted blocks. The first series of materials, illustrated in Figure 1a, has monodisperse PB backbones and one monodisperse PS graft block per branch point. These trifunctional branch points are randomly distributed along the PB backbone and there are, on average, five per molecule. The second series of materials, illustrated in Figure 1b, has monodisperse PB backbones and two monodisperse PS graft blocks per branch point. These tetrafunctional branch points are randomly distributed along the PB backbone and there are, on average, four per molecule. Thus both of these series of materials are graft copolymers with a limited degree of randomness in their molecular architecture. They are a departure from the well-defined molecular architectures which we have studied in previous work on graft copolymer morphology,[1−7] but they are also a logical and important extension of this previous work toward materials of more commercial importance.

Linear AB diblock copolymers and ABA triblock copolymers form different well characterized nanoscale-phase-separated domain morphologies depending on the relative volume fractions of the two block materials. In strongly segregated systems, the type of structure formed is tied to a specific volume fraction dependence which limits the flexibility in designing new materials for new applications. A way to uncouple block copolymer morphology from its rigid dependence on component volume fractions is to introduce another variable into the system by varying molecule architecture in novel ways. One might suppose that a plurality of new block copolymer molecular structures would introduce a plurality of new variables to be considered in the morphological behavior. However, it is our contention that a large number of the possible variations can be represented by a single *molecular asymmetry parameter*. This asymmetry parameter, which we have been developing[1,3−5] as an extension of that proposed by Milner for miktoarm (mixed arm) star architectures,[8] contains a factor describing the conformational asymmetry between the two block materials and another factor describing the asymmetry inherent in the molecular architecture (the way in which component blocks are linked together). The problem is to figure out how to calculate the architectural asymmetry part of the general asymmetry parameter for all the various archi-

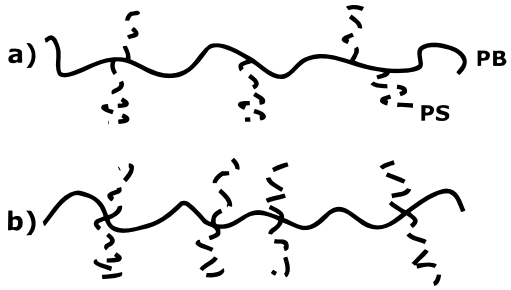

Figure 1. Random multigraft copolymer architectures with (a) trifunctional branch points and (b) tetrafunctional branch points.

[†] University of Athens.
[‡] University of Massachusetts.
[§] Aberdeen Proving Ground.

10.1021/ma980858x CCC: $15.00
Published on Web 10/10/1998

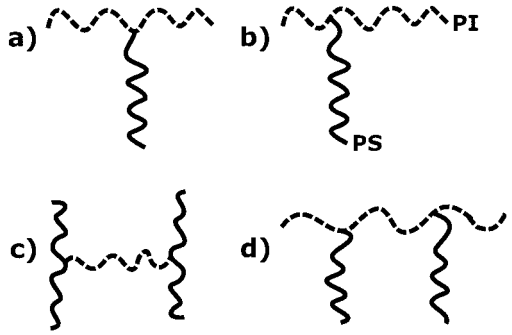

Figure 2. Graft copolymer architectures: (a) single graft, (b) asymmetric single graft, (c) H double graft, and (d) double graft.

tectures encountered. Large molecular asymmetries are accessible by linking common block materials such as PB or polyisoprene (PI) and PS together in graft copolymer geometries. Figure 5c in ref 5 shows a morphology of alternating nanoscale, thick and thin lamella; the volume percents of the dark OsO_4-stained PI domains and the light PS domains are 74% and 26% respectively. This unusual lamellar structure was formed by an H-shaped, S_2IS_2, double graft copolymer.

The overall goal of our graft copolymer research is to systematically build a knowledge of graft copolymer morphological behavior beginning from the very simplest single graft molecules shown in parts a and b of Figure 2. The molecule in Figure 2a has a single PS graft placed in the middle of a PI backbone. Alternatively, this molecule may be interpreted as a three-armed miktoarm star with two PI arms of identical length and one PS arm. We refer to this architecture as the symmetric single graft or I_2S. The architecture in Figure 2b has a single PS graft placed asymmetrically along a PI backbone. In the notation of Olvera de la Cruz and Sanchez,[9] the molecule in Figure 2a corresponds to a single graft structure in which $\tau = 0.5$, where τ is the fractional distance along the PI backbone at which the PS graft occurs. In Figure 2b, τ is not equal to 0.5, and we refer to this type of structure as an asymmetric single graft (ASG). Once we had developed an understanding of the effect of single graft architecture on morphology, the next step was to investigate double graft architectures, two of which are shown in parts c and d of Figure 2. The double graft architectures may be thought of as two single graft molecules linked together in different ways. The architecture in Figure 2c, the H double graft molecule or S_2IS_2, can be imagined as two symmetric single graft molecules linked together at the ends of the grafted blocks, PI in this case. The architecture in Figure 2d, the π double graft molecule or (SI)I((SI), can be imagined as two single graft molecules linked together by the ends of their PI backbones.

To discuss architectural effects on morphology from an overall perspective, we formalize the concept of dividing complex graft architectures of the types shown in Figures 1 and 2c,d into component parts which we will call *constituting block copolymers*. Assuming a lamellar morphology for simplicity, in linear diblock copolymers, each domain consists of two brushes grafted from the two opposite interfaces. Both A and B domains contain free chain ends which are generally clustered near the middle of the domains. For more complicated molecular architectures, "bridges", which are blocks with one end grafted from each of the two opposite interfaces, and "loops", which are blocks with both ends grafted from the same interface, are formed. For example, the B domains of ABA triblock copolymers contain no free chain ends, only loops and bridges. The A domains, by contrast contain only free chain ends. Cutting the loops and bridges in half results in a system consisting of the constituting block copolymers. For example, the symmetric ABA triblock copolymer has $A(^1/_2B)$ as the constituting block copolymer. This notation specifies a diblock copolymer composed of an A block equal to one of the A blocks of the original triblock and a B block equal to half of the B block of the original triblock.

It has been shown by both experiments and theoretical calculations that, for high molecular weights, symmetric ABA triblock copolymers, $(AB)_n$ star copolymers,[10−13] and ...ABAB... infinite multiblock copolymers[14,15] have the same morphology as their *constituting* linear diblock copolymers which are obtained by imagining the molecules to be cut in the middle of all loops and bridges in the morphologies.[1,4,5] The small amount of information that exists for cyclic AB block copolymers suggests that the morphological behavior may also be similar to that of linear constituting diblocks.[16,17] The connections in the microphase separated domains which loops and bridges provide may strongly influence other material properties,[18] but they have only a slight effect on the morphological behavior. The constituting block copolymer of a graft copolymer architecture with trifunctional branch points is an I_2S single graft copolymer or an off-center single graft copolymer[1,4,5] rather than a linear diblock.

The I_2S symmetric single graft structure is a special case of the general A_nB_m miktoarm star architecture. The effect of miktoarm architecture on the volume fraction ranges in which various morphologies are formed was investigated by Milner[8] with a self-consistent field theory in the strong segregation limit ($\chi N > 100$). Connecting different numbers of A and B arms at one junction point creates an asymmetry in the way that the opposing A and B block materials fill space. We define *corresponding block copolymers* to be materials which differ in architecture but have the same overall component volume fractions and total molecular weight. Compared to a corresponding linear diblock, block copolymers with two or more arms on the same side of the interface in a microphase separated structure experience lateral crowding of the multiple blocks. This in turn results in more chain stretching normal to the interface on the side with multiple arms. There is a shift in interfacial curvature preference in order to alleviate this asymmetry in chain stretching: the interface tends to increase in curvature (mean curvature) when viewed from the side of the block material with higher arm number. This statement takes into account the sign convention for interfacial mean curvature, which assigns a negative sign to curvature on the concave side of the interface and a positive sign to curvature on the convex side of the interface.[2,19,20] If the higher arm number occurs on the concave side of the interface, the interface will tend to be less concave (less negative curvature) than it would be in a corresponding linear diblock copolymer. If the higher arm number occurs on the convex side of the interface, then the interfacial curvature will tend to be more convex (more positive curvature) than it would be in a corresponding linear diblock copolymer.[2]

Table 1. Molecular Characteristics of Trifunctional and Tetrafunctional Multigrafts

sample	M_w (PB)[a] ($\times 10^{-3}$)	M_w/M_n (PB)[b]	M_w (PS)[a] ($\times 10^{-3}$)	M_w/M_n (PS)[b]	M_w (RMG)[a] ($\times 10^{-3}$)	M_w/M_n (RMG)[b]	vol % PS[c]	no. of branch points[d]
RMG-3-5-18	198	1.04	10.2	1.04	247	1.06	18.1	4.9
RMG-3-5-34	198	1.04	23.2	1.03	314	1.06	33.7	5.0
RMG-3-5-41	198	1.04	31.4	1.03	353	1.06	40.8	4.9
RMG-3-5-48	198	1.04	41.6	1.04	420	1.06	47.5	5.3
RMG-3-5-62	198	1.04	73.8	1.05	577	1.07	61.6	5.1
RMG-4-4-16	198	1.04	5.5	1.04	245	1.06	16.1	4.3
RMG-4-4-28	198	1.04	11.3	1.03	283	1.05	28.4	3.8
RMG-4-4-43	198	1.04	21.6	1.03	383	1.05	43.1	4.4
RMG-4-4-61	198	1.04	44.5	1.04	554	1.06	60.7	4.0

[a] LALLS in THF at 25 °C. [b] SEC in THF at 30 °C. [c] *Polymer Handbook*. 3rd ed.; Brandrup, J., Immergut, E. H., Eds.; Wiley-Interscience: New York, 1989. [d] Per backbone chain, calculated from M_w values of PB backbones, PS branches, and graft copolymers as determined by LALLS.

These curvature preferences, as illustrated in a mean-field morphology diagram for A_nB_m type block copolymers calculated by Milner, result in a shift of the morphological transition lines toward higher volume fractions of the lower arm number component. In this calculation, the asymmetry caused by the difference in A and B arm numbers was lumped with the conformational asymmetry inherent in the A and B polymer chains into one asymmetry factor, $\epsilon = (n_A/n_B)(l_A/l_B)^{1/2}$. Here (n_A/n_B) is the ratio of arm numbers of the two block types and represents the asymmetry due to the architecture. The conformational asymmetry between the two block materials is expressed by the ratio, $(l_A/l_B)^{1/2}$, where l_i is the ratio of segmental volume to the square of statistical segment length for the block material i.

The I_2S and ASG as well as model double graft copolymer architectures have been experimentally demonstrated to produce a shift in the volume fraction ranges in which the various well-known block copolymer morphologies (A spheres, A cylinders, lamellae, B cylinders, B spheres) are observed to higher volume fractions of the graft block material.[3−6] The results of these studies are in general agreement with the theoretical predictions embodied in the Milner morphology diagram, and they validate the constituting block copolymer concept. Those few samples which do not agree with the predictions of the Milner diagram are part of an overall trend, also observed in I_3S miktoarm stars,[21] indicating a tendency of the Milner morphology diagram to slightly overestimate the shift in volume fraction windows of the various morphologies due to architectural asymmetry.

Graft copolymers have long been of interest as a result of their application as interface compatiblizers in blends. Several studies of graft copolymers have been carried out previously.[22,23] However, previous studies have been limited to samples that have been prepared in similar fashion as those commonly used as blend compatibilizers, which produces a polydisperse sample of ill-defined architecture. More careful synthesis has been performed,[24] but in no case has a systematic attempt been made to elucidate the morphological behavior of this class of copolymer. The present study of the effect on morphology of graft architecture with controlled amounts of randomness is a start in this direction and also is a logical extension of our previous work on more well-defined architectures.

Experimental Section

Synthesis. The random trifunctional and tetrafunctional multigraft copolymers were prepared via anionic polymerization and hydrosilylation chemistry.[25] A study has been carried out involving the hydrosilylation of PB in the presence of platinum divinyltetramethyldisiloxane complex in xylene (Petrarch PC072), which selectively catalyzes the hydrosilylation of the vinyl C═C bonds of the PB.

Table 2. Weight Percent of PS of Trifunctional and Tetrafunctional Multigrafts

sample	wt % PS by ^{1}H NMR[a]	wt % PS by UV−SEC[b]	wt % PS by dn/dc[c]	calcd wt % PS[d]
RMG-3-5-18	21	20	20	20
RMG-3-5-34	37	36	36	37
RMG-3-5-41	44	44	42	43
RMG-3-5-48	50	52	51	53
RMG-3-5-62	64	64	66	66
RMG-4-4-16	17	17	18	19
RMG-4-4-28	29	29	30	30
RMG-4-4-43	45	45	46	48
RMG-4-4-61	62	63	64	64

[a] NMR in $CDCl_3$ at 30 °C. [b] SEC in THF at 30 °C. [c] Calculated from $dn/dc = w(dn/dc)_{PS} + (1 - w)(dn/dc)_{PB}$ using the values of the differential refractive index, dn/dc, of the PS and the PB graft copolymers determined in THF at 25 °C. [d] Calculated from the M_w values of PB backbones, PS branches, and the multigraft copolymers, as determined by LALLS.

The synthetic procedure was based on coupling hydrosilylated PB backbones with living PS arms. The PB backbone and the PS arms were prepared by anionic polymerization[26] using high vacuum techniques in evacuated, *n*-BuLi-washed, and benzene-rinsed reactors. The PB backbone was hydrosilylated with chlorodimethylsilane in the presence of Petrarch PC072 catalyst. The resultant chlorosilylated PB was coupled with living PS. In the case of tetrafunctional multigrafts, dichloromethylsilane was used instead of chlorodimethylsilane. To relieve the steric hindrance and facilitate the addition of two PS arms per branch point, the living arms were capped with three to four units of butadiene before the coupling reaction with the multifunctional backbone. Details are given elsewhere.[25]

Molecular Characterization. The molecular weight distributions and the purities of the final multigrafts were evaluated by size-exclusion chromatography (SEC) at 30 °C. The weight-average molecular weight was determined by low-angle laser light scattering (LALLS) in THF at 25 °C. The compositions of the copolymers were determined by SEC−UV at 260 nm and ^{1}H NMR spectroscopy. The results of these molecular characterization studies are given in Tables 1 and 2. Our nomenclature for these samples gives a rough description of the molecular architecture. In the name RMG-3-5-62, The "RMG" in the first position stands for "random multiple graft," the 3 in the second position indicates that the graft points have a single PS block attached and are thus trifunctional, the 5 in the third position indicates that there are an average of five graft points per PB backbone, and the 62 in the fourth position indicates a total composition of 62 vol % PS. Samples with a 4 in the second position have two PS arms attached at each tetrafunctional branch point. The molecular characterization results conclusively establish that the samples actually possess the predicted architecture and can be char-

Table 3. Morphological Characteristics of Trifunctional and Tetrafunctional Multigrafts

sample	χN(120 °C)	χN(100 °C)	T_g (PS arm) (°C)[a]	χN(T_g PS arm)	χN(25 °C)[a]	d^* (Å)[b]	domain radius (Å)	morphology
RMG-3-5-18	40	42	81	44	52	290	94	PS spheres
RMG-3-5-34	45	47	92	48	59	307	84	PS cylinders
RMG-3-5-41	49	52	94	53	65	369	110	PS cylinders
RMG-3-5-48	51	54	95	55	68	439		lamellae
RMG-3-5-62	67	70	97	71	88	498		lamellae
RMG-4-4-16	22	24	65	26	30	302		disordered
RMG-4-4-28	28	29	83	31	37	341	75	PS cylinders
RMG-4-4-43	29	31	91	32	39	461		lamellae
RMG-4-4-61	41	44	96	44	55	595	130	PB cylinders

[a] T_g of PS arm calculated using the Fox−Flory equation, assuming $M_w = M_n$. [b] Primary SAXS reflection, $d^* = 2\pi/q^*$.

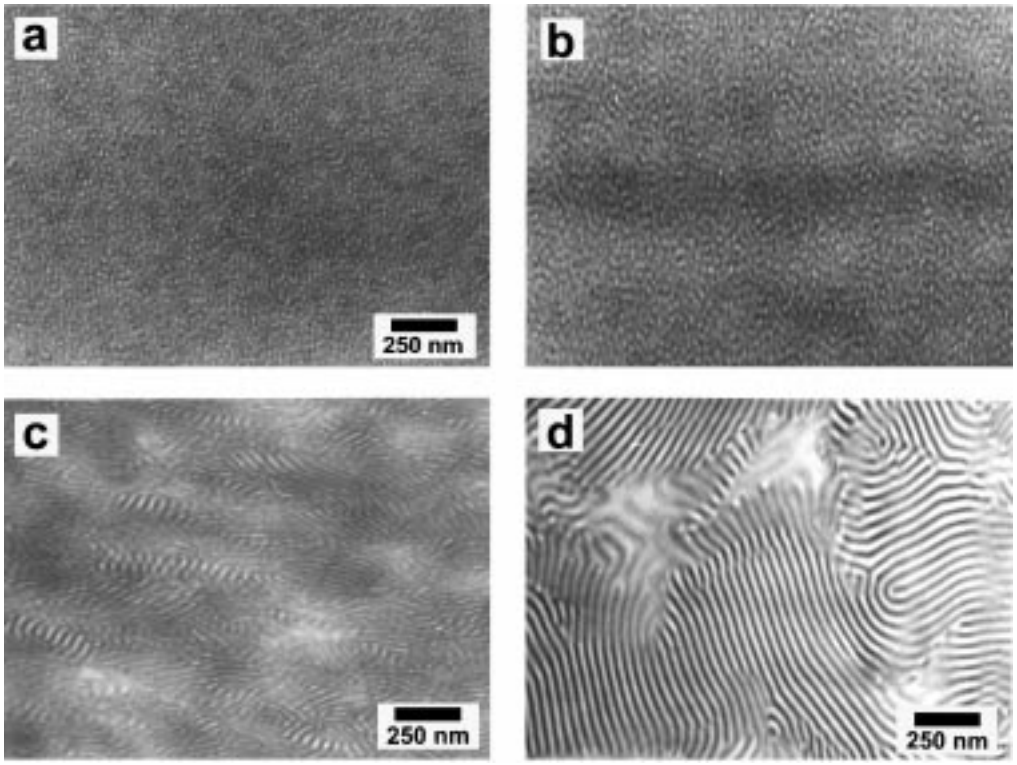

Figure 3. Representative TEM micrographs of (a) RMG-3-5-18, (b) RMG-3-5-41, (c) RMG-3-5-48, and (d) RMG-3-5-62.

acterized as model materials due to their well-defined structures.

Morphological Characterization. Solid films of the graft copolymer material, approximately 2 mm thick were cast from solution in toluene, a nonpreferential solvent for PS and PB, over a period of 2 weeks. In an effort to enhance the development of long range order the samples were thermally annealed at 120 °C under vacuum for 1 week. These casting and annealing conditions have been found to promote self-assembly of well-ordered, nanostructured morphologies in our previous studies of single and double graft copolymers. After annealing, ultrathin sections approximately 500−1000 Å thick were prepared for TEM observation by cryoultramicrotoming. The sections were stained in OsO_4 vapors for about 4 h, to allow TEM imaging of the structures. Small-angle X-ray scattering (SAXS) experiments were also performed in order to determine the lattice symmetries, domain shapes, and spacings of the morphologies. SAXS was performed at the Advanced Polymers Beamline (APB, X27C) at the National Synchrotron Light Source (NSLS), Brookhaven National Laboratory (BNL). The 3 mm^2 beam had a wavelength of 1.307 Å. The camera length was 1.410 m. Two-dimensional scattering patterns were recorded on Fujitsu HR-V image plates and were digitized using a Fujitsu BAS 2000 image plate reader. Background was subtracted, circular averaging was performed, and the data was converted to a log intensity scale in order to generate plots of log I vs q.

Results

The morphological results for the series of materials with an average of five trifunctional branch points per molecule are now presented. The morphological assignments for each sample as well as dimensions determined by SAXS are summarized in Table 3. Figure 3a shows a TEM image for sample RMG-3-5-18, which displays a characteristic microphase separated but disordered morphology. Viewing stereopair images of this structure suggests, although not conclusively, that the structure consists of randomly packed spherical domains. The SAXS for RMG-3-5-18 is shown in Figure 4a along with form factor scattering curves for spherical and cylindrical domains. The initial peak indicates an average intersphere correlation of 290 Å. The scattering vector of the Bragg peak with the lowest scattering angle is referred to as q^*, and q_n are the series of peaks, in order of increasing scattering angle, beginning with q^*. The ratios of q_n/q^* for the series of peaks in a diffraction pattern are characteristic of the lattice symmetry when Bragg scattering is present. The SAXS data for RMG-3-5-18 display a second broad maximum centered at q_n/q^* equal to 2.4, which is not consistent with the symmetries of any of the lattices known to be

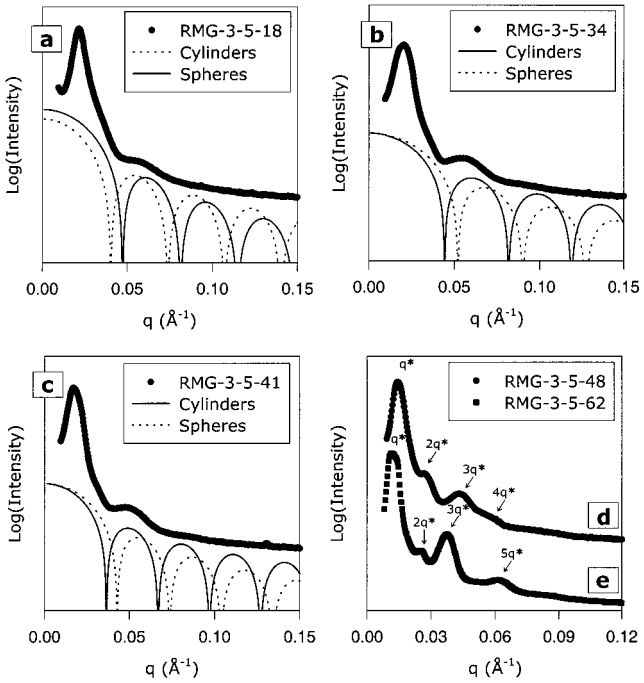

Figure 4. SAXS and form factors for (a) RMG-3-5-18, (b) RMG-3-5-34, (c) RMG-3-5-41, (d) RMG-3-5-48, and (e) RMG-3-5-62.

formed by block copolymers (cubic, hexagonal). This maximum does, however, coincide very well with the second form factor maximum for spherically shaped domains.

To calculate the form factors, we must know the radii of the spherical or cylindrical domains in the morphology. When block copolymer microdomains are well ordered on a lattice, this is best determined from the spacings of the primary scattering peaks. Calculations of domain sizes require the assumption of a lattice packing symmetry and also use the known volume fractions of the two domain materials. Measuring domain sizes on TEM micrographs is generally less desirable due to the possiblities of dimensional changes caused by staining as well as projection artifacts. However, in the present situation, since no lattice is formed, the calculation of domain sizes from a single scattering peak and volume fractions is also approximate. It requires the assumption of some type of lattice order or unit cell as a basis for the calculation. For this reason we have found that more accurate domain dimensions can actually be obtained for the microphase separated but randomly ordered structures in the present study by taking measurements directly from TEM images. Form factors are calculated and compared to the experimental SAXS data for both spheres and cylinders with radii determined from the domain size measured in the micrographs. The spherical form factor gives a better fit to the second broad maximum than the cylindrical form factor calculated for the same (measured) radius. The first minimum of the spherical form factor coincides more accurately with the depression in the scattering curve which precedes (occurs at slightly lower q than) this second maximum. Thus a disordered packing of spherical domains is the structure assigned to RMG-3-5-18. For all samples in this study, the domain radii (spheres or cylinders) upon which the best fit form factor calculations are based are also listed in Table 3.

TEM images of the morphologies for RMG-3-5-34 and RMG-3-5-41 appear nearly identical; only the image for RMG-3-5-41 is shown in Figure 3b. Stereopair TEM images from both these samples suggest a tangle of disordered cylindrical domains of the white PS graft material in a dark PB matrix. The SAXS data for these samples are shown in parts b and c of Figure 4. Both show a strong initial peak and a broad second maximum at scattering vector ratios of 2.3 (RMG-3-5-34) and 2.8 (RMG-3-5-41), which are inconsistent with Bragg scattering. Form factors for cylindrical and spherical domains are also plotted in parts b and c of Figure 4; domain sizes were measured from TEM micrographs as discussed previously. The agreement of the second form factor peak for cylinders with the second broad experimental scattering maximum in both RMG-3-5-34 and RMG-3-5-41 confirms the assignment of a disordered cylindrical morphology to these two samples.

The lamellar morphologies formed by samples RMG-3-5-48 (Figure 3c) and RMG-3-5-62 (Figure 3d) are among the most ordered morphologies displayed by any of the randomly grafted materials in this study. These lamellar phases are, however, clearly much less well ordered than typical lamellae in diblock copolymers or model graft materials of simpler and more regular molecular architecture.[3−6,27,28] The SAXS data for RMG-3-5-48 (Figure 4d) clearly show four Bragg peaks with scattering vector ratios of 1, 2, 3, and 4, consistent with the lamellar morphology. The SAXS data from RMG-3-5-62, shown in Figure 4e, have four distinct Bragg peaks which represent the first, second, third, and fifth orders of the lamellar long period.

The morphological results for the series of materials with an average of four tetrafunctional branch points per molecule are now presented, with quantitative dimensions listed in Table 3. Sample RMG-4-4-16 displays a microphase separated but disordered morphology similar to that observed in previously discussed materials with disordered spherical and cylindrical structures. A TEM image of this sample is shown in Figure 5a, and the SAXS data are shown in Figure 6a. The SAXS data for RMG-4-4-16 show a single maximum falling off slowly at higher scattering angle. This scattering, coupled with the placement of this sample at the ODT (described in the Discussion), suggests that the morphology consists of immobilized and stained composition fluctuations. It is interesting to note that the TEM image of these composition fluctuations is not much different from the images produced by more strongly segregated spherical and cylindrical samples which lack lattice symmetry. Only from the scattering data can one tell the difference.

The TEM image of RMG-4-4-28 (Figure 5b) shows a similar microphase separated structure with a lack of lattice ordering. The SAXS data for this sample (Figure 6b) show the primary peak, a broad shoulder around q of 0.04, and another broad maximum at q of about 0.07. These features can be attributed to the form factor for a cylindrical domain shape. Sample RMG-4-4-43 displays a lamellar morphology with considerably greater long range order than the other samples in this series. This can be seen in the TEM image in Figure 5c. The SAXS data for this sample (Figure 6c) show four peaks consistent with the first, second, fourth, and fifth orders of the lamellar long period. In TEM (Figure 5d), sample RMG-4-4-61 shows a microphase-separated but poorly ordered morphology which displays some small regions

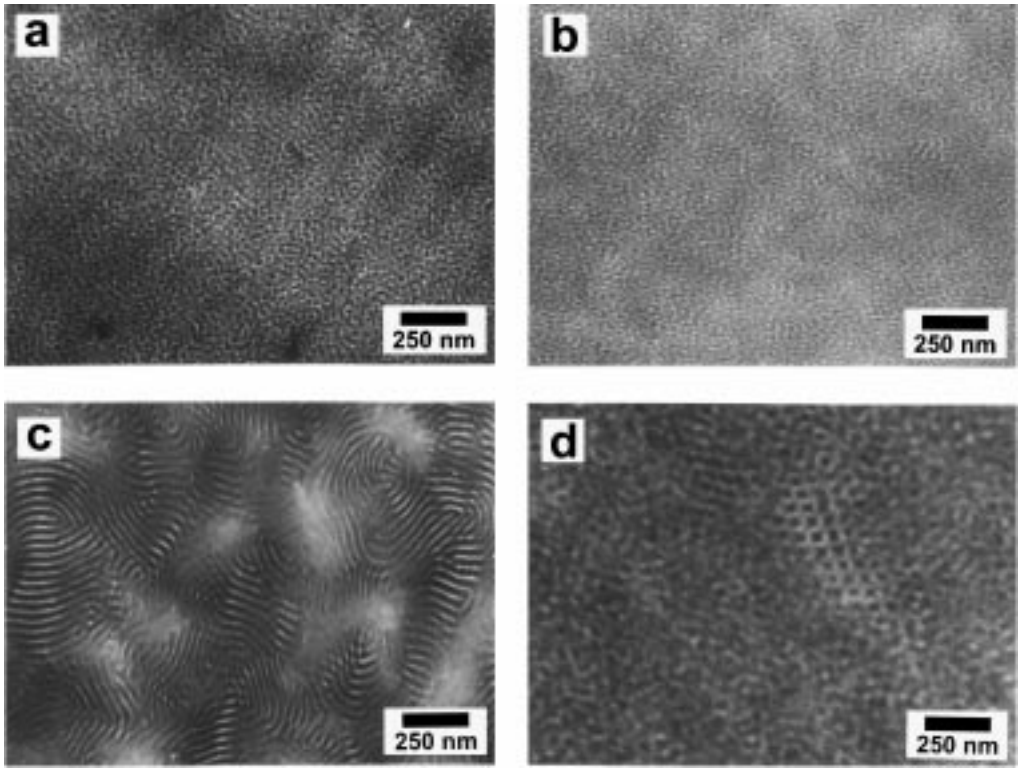

Figure 5. Representative TEM micrographs of (a) RMG-4-4-16, (b) RMG-4-4-28, (c) RMG-4-4-43, and (d) RMG-4-4-61.

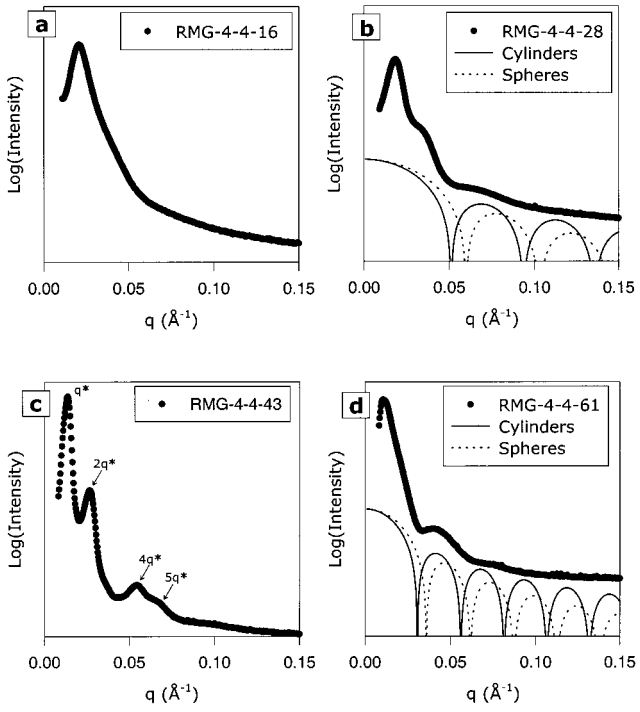

Figure 6. SAXS and form factors for (a) RMG-4-4-16, (b) RMG-4-4-28, (c) RMG-4-4-43, and (d) RMG-4-4-61.

of limited lattice-like order. The SAXS data for this sample (Figure 6d) show a primary peak and a second broad maximum which correlates well with the second maximum of the cylinder form factor.

Discussion

The fact that the random multigraft copolymer materials investigated in this study exist in the intermediate and weak segregation regimes at the conditions under which they were annealed and then observed complicates the interpretation of the results as compared with our previous studies of more strongly segregated model graft copolymers.[1,3−7] The Milner morphology diagram onto which we have mapped the constituting single graft copolymers in these previous studies is only strictly applicable to strongly segregated materials. Calculations of intermediate segregation morphological behavior of diblock copolymers have been carried out by Vavasour and Whitmore,[29] Matsen and Schick,[30] Lescanec and Muthukumar,[31] and Matsen and Bates.[32] However, these theories have not been extended to graft molecular architectures. We can, however, still use what theoretical work does exist as an approximate guide for interpreting the current experimental results.

Our results point to the importance of the constituting graft copolymer concept in determining the effect of graft molecular architecture on both the morphology and the degree of segregation. The RMG-3-5 series is the more strongly segregated set of samples in this study, based on χN values calculated for the average constituting block copolymers. The theoretical work of Balazs and co-workers[33] indicates that it is the χN of the average constituting single graft copolymer which determines the proximity to the ODT. These χN values are listed in Table 3 for three different temperatures: 120 °C (annealing temperature), 100 °C (T_g of bulk PS), and 25 °C (room temperature). The value of χ as a function of temperature for PS and PB was obtained from the work of Wolff et al.[34] Since after annealing the samples were slowly cooled to room temperature over the course of about a day, it is suspected that the degree of segregation at the temperature where the PS domains approach T_g is the most relevant to the morphology which we observe. The T_g of bulk PS at high molecular weight is about 100 °C and thus values for this temperature are included in the table. Additionally, T_g of PS in small microphase-separated

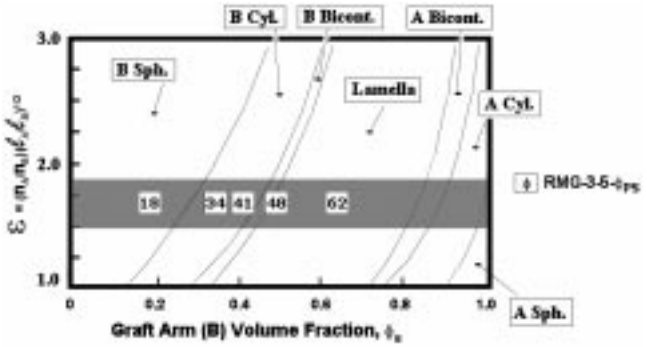

Figure 7. Milner morphology diagram with RMG-3-5 series samples plotted assuming an A_2B constituting block copolymer. The shaded band indicates the range of molecular asymmetries, ϵ, in agreement with morphological characterization. The box symbols map the RMG-3-5 samples onto the diagram; the numbers in the boxes are the volume percent PS in these samples.

domains may be different from that of bulk PS. The fact that some of the PS graft block molecular weights are quite low (around 5000−10,000) will lead to a suppression of T_g as given by the Fox−Flory equation.[35] The PS T_g values calculated with this equation as well as the corresponding χN values are also listed in Table 3. It is apparent that T_g suppression due to low molecular weight does not significantly increase χN over the value at 100 °C. Low molecular weight may not, however, be the only factor influencing T_g of the PS domains. Confinement effects, interfacial energy and perturbed chain conformation may all effect the T_g of PS in these microphase separated systems. These effects are not currently well understood, and thus we will proceed using χN values at 100 °C.

At 100 °C, χN ranges from 39 for RMG-3-5-18 to 68 for RMG-3-5-62. Unfortunately the only theories we have for comparison are the strong segregation calculations of Milner[8] for miktoarm stars and the weak segregation calculations of the order−disorder transition for A_2B single grafts (Olvera de la Cruz and Sanchez[9] and Floudas *et al.*[36]) and comb-shaped multiple graft copolymers (Balazs and co-workers[33]). Calculations of the ODT and order−order transitions for model star and multiple graft copolymers by Dobrynin and Erukhimovich[37] are unfortunately confined to the weak segregation region. Of these theories, only the Milner calculation provides for any comparison to the morphologies actually formed. The other theories are, however, useful in that they allow us to estimate the strength of microphase separation in grafted morphologies by how far they are above the ODT. The calculations of Olvera de la Cruz and Sanchez[9] and Floudas *et al.*[36] indicate that in the A_2B architecture with a graft (B block) volume fraction of 0.2 that the ODT is shifted upward to a χN value of about 32.5, placing sample RMG-3-5-18 in a weakly segregated state. All the other RMG-3-5 samples have degrees of segregation in the intermediate regime.

Figure 7 shows the Milner morphology diagram with symbols plotted at the volume fractions of the PS grafts corresponding to the samples in the RMG-3-5 series. We are unsure of the value of the molecular asymmetry parameter, ϵ, which is appropriate for our materials. The conformational asymmetry between the PS and PB block materials may be relatively strong, about 0.6.[29] We assume an average constituting block obtained by assigning a single PS graft to the average length of backbone obtained by dividing the total backbone length by the average number of grafts per molecule. It is unclear whether this average constituting graft copolymer should be considered symmetric ($\tau = 0.5$) or asymmetric. If it is symmetric, then $\epsilon = 2 \times 0.6 = 1.2$. Otherwise, $\epsilon = f(\tau) \times 0.6$, where τ represents the appropriate average asymmetry in the constituting graft copolymer, and $f(\tau) \leq 2$.[1,3,4] The data for all the samples agree with the diagram in a band ranging between ϵ values of about 1.5 and 1.7, which is shaded on the diagram. Any quantitative comparison is fraught with uncertainty resulting from the error inherent in our composition information about the graft copolymers, our estimation of χN, our estimation of the conformational asymmetry, and the application of a strong segregation diagram to intermediately segregated polymers. However, it is clear that there is a morphological shift brought about by the random graft architecture. Samples RMG-3-5-18, RMG-3-5-34, and RMG-3-5-44 display morphologies which are shifted from those of diblock copolymers or other symmetric molecular architectures at the same composition. We should, however, keep in mind that intermediate segregation is likely to shift all the order−order transition lines in the Milner diagram closer to the center of the diagram as is the case in morphology diagrams calculated for simpler molecular architectures in intermediate segregation.[29,30,32] Thus, the order−order transitions on the left side of the Milner diagram, which impact on the morphologies of the RMG-3-5 series, will be shifted slightly to the right. This would shift the range of agreement with experiment to slightly lower ϵ values.

The RMG-4-4 series is less strongly segregated, as can be appreciated by both the calculated χN values and by the morphological results. The average constituting graft copolymers for this series are A_2B_2 stars and the spinodal curves for materials of general A_nB_n architecture have been calculated by Olvera de la Cruz and Sanchez.[9] In this calculation they use the degrees of polymerization of only a single A and a single B block to calculate χN. Application of this χN calculation to the RMG-4-4 series results in values at 100 °C ranging from 24 to 42. Comparison of Figures 3 and 5 in ref 9 suggests that the morphological behavior of the A_2B_2 molecules is quite similar to that of simple AB diblocks. This conclusion agrees with the fact that both types of molecules are architecturally symmetric as opposed to asymmetric architectures with trifunctional branch points.

Because of this similarity and because weak and intermediate segregation calculations of order−order transitions are not available for the A_2B_2 architecture of our constituting graft copolymer, we make an approximate comparison of our experimentally observed morphologies with the weak and intermediate segregation results calculated by Vavasour and Whitmore for conformationally asymmetric AB diblock copolymers.[29] Similar morphology diagrams including the gyroid morphology have been calculated by Matsen and Schick[30] and Matsen and Bates.[32] However, since we cannot definitively identify any bicontinuous morphologies, we use the diagram of Vavasour and Whitmore which includes only spheres, cylinders, and lamellae. Figure 8 shows the experimental points of the RMG-4-4 series plotted on the morphology diagram calculated by Vavasour and Whitmore for a conformational asymmetry of 0.6. Here f_A must be used to refer to the PB volume fraction. This conformational asymmetry closely matches

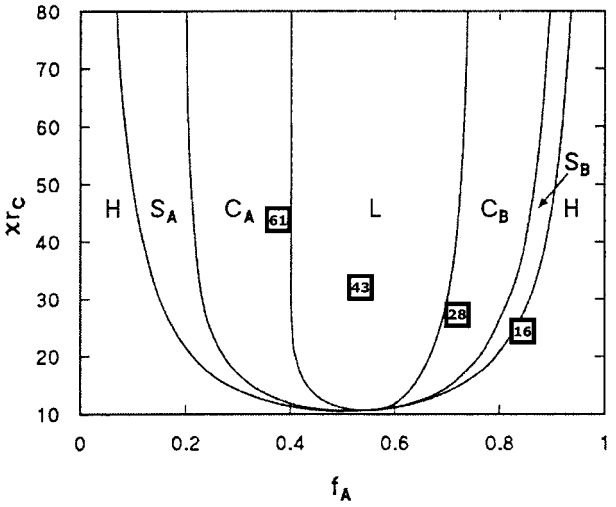

Figure 8. Morphology diagram from Vavasour and Whitmore, including RMG-4-4 series samples, plotted assuming a linear diblock constituting a block copolymer.

that which as been reported for the PS−PB block materials.[29] The architectural asymmetry (n_A/n_B) for the PS_2PB_2 constituting architecture is unity. The experimental observation that sample RMG-4-4-16 produces a chaotic morphology with no long range order and no characteristic domain shape is consistent with the placement of the average constituting graft copolymer for this material close to, but below the ODT. Samples RMG-4-4-28 and RMG-4-4-43 were observed to form disordered cylinders and lamellae respectively, in agreement with their placement on the morphology diagram. Finally, sample RMG-4-4-61, at 61 vol % PS, maps onto the cylinder region of the morphology diagram, again in agreement with our experimental findings. A conformationally symmetric diblock or A_2B_2 architecture at this composition would be lamellar. The fact that we observe cylinders is a manifestation of the effect of the PS−PB conformational asymmetry.

It is interesting to compare the effect of graft molecular architecture on the degree of segregation for the trifunctional branch points of the RMG-3-5 series and the tetrafunctional branch points of the RMG-4-4 series. The work of Olvera de la Cruz and Sanchez[9] tells us that the appropriate way to calculate χN for A_2B architectures is based on the total degree of polymerization of both A arms and the B arm. For A_2B_2 architectures, χN is calculated based on one arm of each material, i.e., based on the A_1B_1 diblock. This leads to significantly lower values of χN for graft copolymers with tetrafunctional branch points, as compared to materials of the same composition and total molecular weights of both A and B components but with trifunctional branch points. An experimental verification of this effect can be appreciated by comparing the χN values for pairs of samples, one from the RMG-3-5 series and one from the RMG-4-4 series, which have the same overall volume fractions and approximately the same total amount of PS grafted at each junction point. The following pairs of samples permit such a comparison: (RMG-3-5-18 and RMG-4-4-16), (RMG-3-5-34 and RMG-4-4-28), and (RMG-3-5-41 and RMG-4-4-43). The χN values for the samples with tetrafunctional branch points are about 40% lower than those of the corresponding materials with trifunctional branch points. Olvera de la Cruz and Sanchez show that the ODT occurs at slightly higher values of χN for materials with trifunctional branch points, an increase from 10.5 to 13.5 at 0.5 volume fraction. However, this does not compensate for the difference in χN between trifunctional and tetrafunctional branch points. The good agreement of the data from our series of samples with tetrafunctional branch points with the weak and intermediate segregation predictions of Vavasour and Whitmore supports the application of the constituting graft copolymer approach to our materials as well as the calculation of χN for these constituting block copolymers using the procedures of Olvera de la Cruz and Sanchez.

Conclusions

In general the morphological characterization results for all the series of samples indicate little or no long range order for materials displaying spherical and cylindrical morphologies. The order is slightly better for materials giving lamellar morphologies. This lack of long range order is undoubtedly the result of two factors. First, the relatively high molecular weight and multiple junction points of these materials must severely limit the molecular mobility necessary to increase long range order during solvent casting and thermal annealing. Second, the architectural dispersity of the molecule resulting from random graft point locations along the backbone causes different parts of the molecule to locally prefer a different morphology than other parts of the same molecule which by chance have a different local graft density. Our results indicate that the molecules form the morphologies which are dictated by their average constituting single graft copolymer structures. However, the *multiple personalities* inherent in the different local parts of the molecular architecture lead to significant suppression of long range order.

Even with the loss of long range order, the samples, as a function of average molecular architecture (i.e. junction point density) and composition, do show a clear preference for a specific domain shape (spherical, cylindrical, or lamellar). In disordered cylindrical morphologies, it sometimes appears that the cylinders have a tendency to form three way branch points, and thus some of these structures may be more properly categorized as disordered bicontinuous structures. However, the differentiation of disordered cylinders and disordered bicontinuous structures is nearly impossible based on the projected images in TEM micrographs and on the scattering data. Essentially all that remains when long range order is reduced or lost entirely is the general domain shape. This is expressed as the preference for domain dimensionality: spheres 0, disordered cylinders 1, and lamellae 2.

The lamellar domain shape, when formed, appears to require the establishment of at least a modest degree of long range order. A similar degree of lattice order does not appear to be required for the formation of spherical and cylindrical domains. This result can be simply understood in terms of the excluded volume characteristics of the spherical, cylindrical and lamellar domain shapes. Because lamellae extend over two spatial dimensions, they must pack parallel to one another or they cannot fill space to the density required of these materials. Essentially the lamellar domain shape templates its own long range order. Spherical and cylindrical domains have more freedom to form disordered packings while still filling space to uniform density.

Acknowledgment. S.P.G. and F.L.B. acknowledge funding from the U. S. Army Research Office (ARO) under Contract DAAG55-98-1-0116. N.H. and M.X. wish to acknowledge the Greek General Secretariat of Research and Technology and the Research Committee of the University of Athens for financial support. Helpful discussions with Dr. J. Roovers are gratefully acknowledged by M.X. and N.H. We acknowledge the use of instruments in the W. M. Keck Electron Microscopy Laboratory, and Central Facility Support from the Materials Research Science and Engineering Center (MRSEC), both at the University of Massachusetts Amherst. We wish to acknowledge Prof. Benjamin Hsiao and Dr. F.-J. Yeh for their help in using the equipment and software at the Brookhaven beamline. We also acknowledge useful discussions regarding the interpretation of the results with Dr. Chin Lee.

References and Notes

(1) Gido, S. P.; Lee, C.; Pochan, D. J.; Pispas, S.; Mays, J. W.; Hadjichristidis, N. *Macromolecules* **1996**, *29*, 7022.
(2) Gido, S. P.; Wang, Z.-G. *Macromolecules* **1997**, *30*, 6771.
(3) Lee, C.; Gido, S. P.; Pitsikalis, M.; Mays, J. W.; Beck Tan, N.; Trevino, S. F.; Hadjichristidis, N. *Macromolecules* **1997**, *30*, 3732.
(4) Lee, C.; Gido, S. P.; Poulos, Y.; Hadjichristidis, N.; Beck Tan, N.; Trevino, S. F.; Mays, J. W. *Polymer* **1998**, *39*, 4631.
(5) Lee, C.; Gido, S. P.; Poulos, Y.; Hadjichristidis, N.; Beck Tan, N.; Trevino, S. F.; Mays, J. W. *J. Chem. Phys.* **1997**, *107*, 6460.
(6) Pochan, D. J.; Gido, S. P.; Pispas, S.; Mays, J. W.; Ryan, A. J.; Fairclough, J. P. A.; Hamley, I. W.; Terrill, N. J. *Macromolecules* **1996**, *29*, 5091.
(7) Pochan, D. J.; Gido, S. P.; Pispas, S.; Mays, J. W. *Macromolecules* **1996**, *29*, 5099.
(8) Milner, S. T. *Macromolecules* **1994**, *27*, 2333.
(9) Olvera de la Cruz, M.; Sanchez, I. C. *Macromolecules* **1986**, *19*, 2501.
(10) Matsen, M. W.; Schick, M. *Macromolecules* **1994**, *27*, 6761.
(11) Herman, D. S.; Kinning, D. J.; Thomas, E. L.; Fetters, L. J. *Macromolecules* **1987**, *20*, 2940.
(12) Kinning, D. J.; Alward, D. B.; Thomas, E. L.; Fetters, L. J.; Handlin, D. J., Jr. *Macromolecules* **1986**, *19*, 1288.
(13) Thomas, E. L.; Alward, D. B.; Kinning, D. J.; Martin, D. C.; Handlin, D. L., Jr.; Fetters, L. J. *Macromolecules* **1986**, *19*, 2197.
(14) Matsen, M. W. *J. Chem. Phys.* **1995**, *102*, 3884.
(15) Matsen, M. W.; Schick, M. *Macromolecules* **1994**, *27*, 7257.
(16) Lescanec, R. L.; Hajduk, D. A.; Kim, G. Y.; Gan, Y.; Yin, Y.; Gruner, S. M.; Hogen-Esch, T. E.; Thomas, E. L. *Macromolecules* **1995**, *28*, 3485.
(17) Marko, J. F. *Macromolecules* **1993**, *26*, 1442.
(18) Watanabe, H. *Macromolecules* **1995**, *28*, 5006.
(19) Safran, S. A. *Statistical Thermodynamics of Surfaces, Interfaces, and Membranes*; Addison-Wesley: Reading, MA, 1994; Vol. 90.
(20) Gido, S. P.; Thomas, E. L. *Macromolecules* **1994**, *27*, 849.
(21) Tselikas, Y.; Iatrou, H.; Hadjichristidis, N.; Liang, K. S.; Mohanty, K.; Lohse, D. J. *J. Chem. Phys.* **1996**, *105*, 2456.
(22) Dozier, W. D.; Thiyagarajan, P.; Peiffer, D. G.; Rabeony, M.; Lin, M. Y.; Agrawal, G.; Wool, R. P. *Polymer* **1994**, *35*, 3116.
(23) Price, C.; Singleton, R.; Woods, D. *Polymer* **1974**, *15*, 117−118.
(24) Evans, D. C.; George, M. H.; Barrie, J. A. *Polymer* **1975**, *16*, 690.
(25) Xenidou, M.; Hadjichristidis, N. *Macromolecules* **1998**, *31*, 5690.
(26) Iatrou, H.; Hadjichristidis, N. *Macromolecules* **1993**, *25*, 4649.
(27) Pochan, D. J.; Gido, S. P.; Zhou, J.; Mays, J. W.; Whitmore, M.; Ryan, A. J. *J. Polym. Sci., Polym. Phys.* **1997**, *35*, 2629.
(28) Gido, S. P.; Gunther, J.; Thomas, E. L.; Hoffman, D. *Macromolecules* **1993**, *26*, 4506.
(29) Vavasour, J. D.; Whitmore, M. D. *Macromolecules* **1993**, *26*, 7070.
(30) Matsen, M. W.; Schick, M. *Phys. Rev. Lett.* **1994**, *72*, 2660.
(31) Lescanec, R. L.; Muthukumar, M. *Macromolecules* **1993**, *26*, 3908.
(32) Matsen, M. W.; Bates, F. S. *Macromolecules* **1996**, *29*, 1091.
(33) Shinozaki, A.; Jasnow, D.; Balazs, A. C. *Macromolecules* **1994**, *27*, 2496.
(34) Wolff, T.; Burger, C.; Ruland, W. *Macromolecules* **1993**, *26*, 1707.
(35) Fox, T. G.; Flory, P. J. *J. Appl. Phys.* **1950**, *21*, 581.
(36) Floudas, G.; Hadjichristidis, N.; Tselikas, Y.; Erukhimovich, I. *Macromolecules* **1997**, *30*, 3090.
(37) Dobrynin, A. V.; Ya. Erukhimovich, I. *Macromolecules* **1993**, *26*, 276.

MA980858X